Polarization-dependent spectra of x-ray dielectronic satellite lines of Be-like Fe

A. S. Shlyaptseva, R. C. Mancini, and P. Neill
Department of Physics, University of Nevada, Reno, Nevada 89557-0058

P. Beiersdorfer, J. R. Crespo López-Urrutia, and K. Widmann
Lawrence Livermore National Laboratory, Livermore, California 94550

(Received 14 August 1997)

We have studied the polarization properties of dielectronic satellite lines in Be-like Fe ions excited through resonant electron capture by an electron beam. Using the photon density-matrix formalism, we have calculated the degree of polarization and polarization-dependent spectra of dielectronic satellite lines, i.e., the spectral intensity distribution of lines associated with a given polarization state. Theoretical results have been compared with experiments performed at the Lawrence Livermore National Laboratory electron-beam ion trap where dielectronic satellite line emission from Fe ions produced at different energies of the electron beam was simultaneously recorded with two crystal spectrometers. These spectrometers had different polarization sensitivities. The experimental spectra recorded by the two spectrometers are reproduced by the theory. This ability to model the polarization dependence of x-ray line spectra is important for the diagnosis of electron beams in plasmas. [S1050-2947(98)02302-6]

PACS number(s): 32.30.Rj, 32.70.Fw, 34.80.Lx, 95.30.Ky

I. INTRODUCTION

X-ray line spectroscopy is an important tool for the diagnosis of space and laboratory plasmas. Most of the spectroscopic diagnostics developed for plasmas have been based on properties of line intensity distributions and line profiles. However, for the case of nonequilibrium plasmas whose electron distribution functions can show different degrees of anisotropy and even the presence of electron beams, the polarization of x-ray line emission can be particularly useful for spectroscopic diagnostic applications. During the past few years electron kinetics simulations of laser-produced plasmas driven by ultrashort (subpicosecond), high-intensity laser pulses have been done using particle-in-cell codes [1–3], Fokker-Planck [4], and Vlasov models [5]. These studies show anisotropic, electron distribution functions for the plasma and the presence of beams of energetic electrons that can carry a substantial amount of the total energy deposited by the laser. Also, the production and characterization of energetic electrons play a critical role in the recently proposed fast ignitor concept where suprathermal electrons produced by ultrahigh-intensity lasers ignite a fuel capsule originally compressed in a conventional laser-driven implosion [6]. New spectroscopic diagnostics leading to the characterization of beams of electrons in plasmas are needed in these areas. Electron beams represent an anisotropic excitation mechanism that results in the emission of partially polarized x-ray lines. In this connection, x-ray line polarization spectroscopy can help to diagnose electron beams in plasmas and to bridge the gap between electron kinetics simulations and experimental measurements.

To our knowledge, the first theoretical investigations of polarization of x-ray line radiation applied to the diagnosis of high-temperature plasmas were done by Haug [7,8] for the case of solar plasmas. In his work, the degree of polarization of resonance lines in H- and He-like Fe ions excited by an electron beam was calculated using the results for polarization of electric-dipole transitions in neutral atoms excited by electron impact from Ref. [9]. Few theoretical and experimental studies have been done on x-ray line polarization. In theoretical studies, two basic excitation mechanisms have been considered: electron-impact excitation and dielectronic recombination. Calculations of the polarization of radiation driven by electron-impact excitation have been made for H-, He-, and Li-like ions in the nonrelativistic [10–14] and relativistic approximations [15,16]. Polarization of dielectronic satellite lines has been considered for H-, He-, and Li-like ions in the nonrelativistic [12,13,17] and relativistic approximations [18]. Also, polarization of dielectronic satellite lines of B-like ions has been computed in the nonrelativistic approximation [19]. In laboratory plasmas, the polarization of x-ray line emission of multiply charged Fe ions in plasmas produced by pulsed, high-current z-pinch discharges has been detected and associated with the presence of suprathermal electrons along the discharge axis [20]. More recently, observations of polarization of x-ray lines excited by electron impact were made in laser-produced plasmas for He-like Al ions by Kieffer *et al.* [21,22], at the Lawrence Livermore National Laboratory (LLNL) electron-beam ion trap (EBIT) for He-like Sc ions by Henderson *et al.* [23] and for He- and Li-like Fe ions by Beiersdorfer *et al.* [24,25], and at the National Institute of Standards and Technology EBIT for Ne-like Ba ions by Takács *et al.* [26]. The EBIT is a powerful tool capable of creating very highly charged ions for atomic structure, electron-ion interactions, and other spectroscopic studies [27]. Various techniques have been demonstrated to measure electron-impact excitation [28] and dielectronic recombination cross sections [29]. Furthermore, the EBIT facility offers an excellent opportunity to observe polarization effects in x-ray line emission in experiments performed under well-controlled conditions. In turn, these measurements can be used to make detailed comparisons with theoretical calculations before applying them to the analysis of polarized spectra from complicated systems such as plasmas.

We have published preliminary results on polarization-dependent spectra of dielectronic satellite lines of Li- and Be-like Fe ions elsewhere [30]. In this paper, we develop and extend our previous study and present an extensive analysis of polarization-dependent spectra of dielectronic satellite lines of Be-like Fe. Theoretical and experimental results of the polarization properties of spectral features formed by the overlapping and blending of dielectronic satellite lines are discussed in detail. This is different from previous investigations on x-ray line polarization, which have focused on the study of the degree of polarization or angular distribution of x-ray emission of single, well-resolved lines. The calculation of polarization-dependent spectra represents a suitable way to study the polarization properties of complex spectra. We have calculated polarization-dependent spectra of dielectronic satellite lines of Be-like Fe and compared them with experimental spectra observed at the LLNL EBIT. To this end, dielectronic satellite spectra were simultaneously recorded with two crystal spectrometers, which acted as polarizers by selectively reflecting polarization states associated with directions parallel and perpendicular to the electron-beam axis. The dielectronic satellite spectrum is significantly polarized and, in general, the two polarization-dependent spectra have different intensity distributions. The details of these spectra also depend strongly on the energy of the electron beam. In Sec. II we develop our theoretical approach for the calculation of polarization-dependent spectra of dielectronic satellite lines; in Sec. II A we present the basic formalism, in Sec. II B we discuss the results of the calculations of atomic and polarization characteristics, and in Sec. II C we display theoretical, polarization-dependent spectra. Experimental details and measurements are given in Sec. III. In Sec. IV we discuss the experimental and theoretical results and their comparison. Finally, in Sec. V we present our conclusions.

II. THEORETICAL APPROACH

A. Formalism

1. Intensities of lines associated with different polarization states

The degree of polarization of line transitions excited by an electron beam observed in a direction perpendicular to the electron beam is defined as

$$P_0=\frac{I_\parallel-I_\perp}{I_\parallel+I_\perp}, \tag{1}$$

where $I_\parallel, I_\perp$ are the intensities associated with electric vectors polarized parallel and perpendicular to the electron beam, respectively. If θ is the angle between the axis of the electron beam and the direction of observation, the total intensity observed at $\theta=90°$ is

$$I(90°)=I_\parallel+I_\perp . \tag{2}$$

For the electric-dipole radiation considered in this paper $I(90°)$ is given by [9]

$$I(90°)=\frac{3}{3-P_0}\langle I\rangle, \tag{3}$$

where $\langle I\rangle$ is the 4π-averaged intensity. Using Eqs. (1)–(3) the intensities associated with each polarization state can be written down in the form

$$I_\parallel=\frac{3}{2}\langle I\rangle\frac{1+P_0}{3-P_0}, \tag{4}$$

$$I_\perp=\frac{3}{2}\langle I\rangle\frac{1-P_0}{3-P_0}. \tag{5}$$

For any dielectronic satellite s, $\langle I\rangle$ can be expressed in terms of the intensity factor $Q_d(s)$, the distribution function of electron energies $f(E)$, and the autoionization energy $E_a(s)$ [29,31]:

$$\langle I(s)\rangle=K_1 f(E=E_a(s))Q_d(s). \tag{6}$$

Here K_1 represents a factor involving fundamental constants and the total electron number density (i.e., factors independent of the type of dielectronic satellite transition in a given ion). We will normalize the values of $\langle I(s)\rangle, I_\parallel$, and $I_\perp$ to K_1. We characterize the beam of electrons with a Gaussian distribution function centered at the beam energy E_b and with a width ΔE. In principle, we can use any other distribution function. In our case, this particular choice is motivated by the fact that it represents a good approximation to the energy distribution of the EBIT electron beam and it is thus suitable for comparing theoretical results with experimental data recorded at the EBIT. Making use of Eqs. (4)–(6), the intensities of dielectronic satellite lines associated with different polarization states have the form

$$I_\parallel=\frac{3}{2}Q_d(s)\exp(-\{[E_b-E_a(s)]/\Delta E\}^2)\frac{1+P_0}{3-P_0}, \tag{7}$$

$$I_\perp=\frac{3}{2}Q_d(s)\exp(-\{[E_b-E_a(s)]/\Delta E\}^2)\frac{1-P_0}{3-P_0}. \tag{8}$$

Thus to calculate the intensity of a dielectronic satellite line s associated with parallel and perpendicular polarization states we need to know the atomic characteristics $Q_d(s)$ and $E_a(s)$ and the degree of polarization of each satellite line $P_0(s)$.

2. Degree of polarization of dielectronic satellite lines

To describe the polarization properties of dielectronic satellite line emission we use the representation of the total momentum of the system. The initial state is characterized by the index i, the target ion in the initial state (before recombination), and the incident electron. The final state is characterized by the index f, the target ion in the final state (after recombination and emission of the photon), and the emitted photon. The quantization axis z is taken along the direction of the electron beam. The cross section for capture of an electron with energy $E=\frac{1}{2}v^2$ (a.u.) is equal to (see, for example, [32])

$$\sigma_{if}=\frac{1}{2g_i}\frac{4\pi^3}{v^2}\sum_k |T_k|^2. \tag{9}$$

Here g_i is the statistical weight of the target ion i; the sum Σ_k denotes the summation over all quantum numbers of the system that characterize the initial and final states, which will be discussed below. The T matrix elements in Breit-Wigner form are given by

$$T_{if}=K_2\sum_a \frac{U_{if}^a}{E-E_{ai}+\frac{1}{2}jA_a}, \tag{10}$$

where K_2 is a factor involving fundamental constants, a denotes autoionization levels, j is the imaginary unit, E_{ai} is the energy of the nonradiative transition $a\rightarrow i$, and A_a is the natural width of the level including radiation and autoionization widths. U_{if}^a is the matrix element associated with the interaction operator $\hat{U}^a$, which is determined by the electron-electron electrostatic interaction operator $\hat{U}^e$ and the electron-electromagnetic field interaction operator $\hat{U}^{ph}$:

$$\hat{U}_{if}^a=\hat{U}^e(i|a)\hat{U}^{ph}(a|f). \tag{11}$$

The rate per unit of volume at which electron capture occurs in state f is equal to

$$R(f)=\sum_i N_e N_i \int v\sigma_{if} f(E)dE, \tag{12}$$

where N_e is the electron density and N_i is the population density of initial target ions.

The polarization properties of the system can be described by the following density matrix of the system in the final state:

$$W_{f,f'}=\langle M_{J_f};\mathbf{k}\lambda|\hat{U}^a|M_{J_f'};\mathbf{k}\lambda'\rangle. \tag{13}$$

J_f, M_{J_f} are the total momentum of the target ion in the final state and its z projection, $\mathbf{k}$ is the photon direction of propagation, and λ is the helicity of the photon ($\lambda,\lambda'=\pm 1$). The diagonal elements of this density matrix are equal to the rate $W_{f,f}=R(f)$. After integrating over the energy distribution function of the electrons and taking into account the resonance nature of the electron capture process, the nondiagonal elements can be expressed in the form [17,32]

$$W_{f,f'}=\sum_{a,a'} \frac{G_{aa'}}{A_{aa'}}\langle U_{if}^a U_{if'}^{a'*}\rangle, \tag{14}$$

where $G_{aa'}$ characterizes the degree of overlapping of the autoionization levels and is equal to

$$G_{aa'}=\frac{A_{aa'}^2}{A_{aa'}^2+(E_a-E_{a'})^2}, \tag{15}$$

where $A_{aa'}=\frac{1}{2}(A_a+A_{a'})$. If the resonances do not overlap, then $a=a'$, $A_{aa'}=A_a$, and $G_{aa'}=1$.

The polarization properties of partially polarized radiation can be described by the photon density matrix $W_{\lambda,\lambda'}$, which represents the density matrix of the final state summed up over the z projection of the total angular momentum of the ion in the final state [33]:

$$W_{\lambda,\lambda'}=\sum_{M_{J_f}} W_{f,f'}=\sum_{M_{J_f}} \langle M_{J_f};\mathbf{k}\lambda|\hat{U}^a|M_{J_f};\mathbf{k}\lambda'\rangle. \tag{16}$$

At this point it is convenient to introduce the photon density matrix ρ^{ph},

$$\rho_{\lambda,\lambda'}^{ph}=\frac{W_{\lambda,\lambda'}}{\sum_\lambda W_{\lambda\lambda}}, \tag{17}$$

which is normalized to

$$\mathrm{tr}\rho=\rho_{1,1}+\rho_{-1,-1}=1 \tag{18}$$

and using Eqs. (14) and (17) is equal to

$$\rho_{\lambda,\lambda'}^{ph}=\frac{\sum_{M_{J_f}}\sum_{a,a'}\frac{G_{aa'}}{A_{aa'}}\langle U_{if}^a(\lambda)U_{if}^{a'*}(\lambda')\rangle}{\sum_\lambda\sum_{M_{J_f}}\sum_a \frac{\langle|U_{if}^a(\lambda)|^2\rangle}{A_a}}. \tag{19}$$

This normalized photon density matrix is very convenient because the elements of $\rho_{\lambda,\lambda'}^{ph}$ do not depend on the electron distribution function $f(E)$, the reduced matrix elements $(i||a),(a||f)$ (as we will see below), or other constants that cancel out in numerator and denominator.

If we introduce partial-wave expansions for the incident electron (sum over l,m_l) and for the photon (sum over j_{ph},m_{ph}), the matrix element $U_{if}^a(\lambda)$ associated with the electron capture $i\rightarrow a$ and subsequent radiation transition $a\rightarrow f$ resulting in a photon with helicity λ can be written as

$$\begin{aligned}U_{if}^a(\lambda)=K_3&\sum_{l,m_l}\sum_{m_s}\sum_{M_{S_i},M_{L_i}}\sum_{M_{S_a}}\sum_{M_{L_a}} i^l e^{i\sigma_l}Y_{lm_l}(\hat{q}_z)\\&\times C^{S_aM_{S_a}}_{\frac{1}{2}M_{S_i}\frac{1}{2}m_s}C^{L_aM_{L_a}}_{L_iM_{L_i}lm_l}C^{J_aM_{J_a}}_{S_aM_{S_a}L_aM_{L_a}}(i||a)\\&\times\sum_{j_{ph},m_{ph}}\sqrt{\frac{2j_{ph}+1}{8\pi}}D^{(j_{ph})}_{\lambda m_{ph}}C^{J_aM_{J_a}}_{J_fM_{J_f}j_{ph}m_{ph}}(a||f).\end{aligned} \tag{20}$$

Here K_3 is a factor involving fundamental constants, σ_l is a Coulomb phase, $\hat{q}_z$ is the angle between the electron beam and the z axis ($\hat{q}_z=0$, in our case), the C symbols represent Clebsch-Gordan coefficients, $(i||a)$ is the reduced matrix element associated with the transition $i\rightarrow a$ relevant to the electron capture process, and $(a||f)$ is the reduced matrix

element associated with the transition $a \rightarrow f$ relevant to the radiative decay process. We describe the initial state of the system in the LS-coupling scheme with the target ion in the initial state characterized by the spin and orbital momenta S_i, L_i and their z projections M_{S_i}, M_{L_i}, and the incident electron characterized by spin z projection m_s, orbital angular momentum l, and its z projection m_l. The autoionization states of the target are characterized by the quantum numbers S_a, L_a, J_a and their z projections $M_{S_a}, M_{L_a}, M_{J_a}$. The target ion in the final state is characterized by J_f, M_{J_f}.

Using Eq. (20) and the contraction of two rotation matrix elements $D^{(j_{ph})}_{\lambda m_{ph}}, D^{(j'_{ph})*}_{\lambda' m'_{ph}}$, we can rewrite the numerator in Eq. (19) in the form

$$\sum_{M_{J_f}} \sum_{a,a'} \frac{G_{aa'}}{A_{aa'}} \langle U^a_{if}(\lambda) U^{a'}_{if}{}^*(\lambda') \rangle = K_3^2 \sum_{J_a, M_{J_a}} \sum_{J'_a, M_{J'_a}} C^{J_a M_{J_a}}_{S_a M_{S_a} L_a M_{L_a}} C^{J'_a M_{J'_a}}_{S'_a M_{S'_a} L'_a M_{L'_a}} \frac{G_{aa'}}{A_{aa'}} (i||a)(i||a')^*(a||f)(a'||f)^*$$

$$\times \sum_{M_{J_f}} \sum_{l, m_l} \sum_{l', m'_l} i^{l-l'} e^{i(\sigma_l - \sigma'_l)} Y_{l m_l}(\hat{q}_z) Y^*_{l' m'_l}(\hat{q}_z)$$

$$\times \sum_{m_s} \sum_{M_{S_i}, M_{L_i}} \sum_{M_{S_a}, M_{S'_a}} \sum_{M_{L_a}, M_{L'_a}} C^{S_a M_{S_a}}_{\frac{1}{2} M_{S_i} \frac{1}{2} m_s} C^{S'_a M_{S'_a}}_{\frac{1}{2} M_{S_i} \frac{1}{2} m_s} C^{L_a M_{L_a}}_{L_i M_{L_i} l m_l} C^{L'_a M_{L'_a}}_{L_i M_{L_i} l' m'_l}$$

$$\times \sum_{j_{ph}, m_{ph}} \sum_{j'_{ph}, m'_{ph}} \frac{\sqrt{(2j_{ph}+1)(2j'_{ph}+1)}}{8\pi} C^{J_a M_{J_a}}_{J_f M_{J_f} j_{ph} m_{ph}} C^{J'_a M_{J'_a}}_{J_f M_{J_f} j'_{ph} m'_{ph}}$$

$$\times (-1)^{\lambda + m_{ph}} \sum_L (2L+1) \begin{pmatrix} j_{ph} & j_{ph} & L \\ \lambda & -\lambda' & -\Lambda \end{pmatrix} \begin{pmatrix} j_{ph} & j_{ph} & L \\ m_{ph} & -m'_{ph} & -\mu \end{pmatrix} D^{(L)}_{\Lambda\mu}. \tag{21}$$

Here indices $\Lambda = \lambda - \lambda'$, $\mu = m_{ph} - m'_{ph}$, and L are integers and $L \leqslant 2j_{ph}$; ( ) are 3-j symbols.

If we assume that the autoionizing states in the Be-like ions are populated by electron capture only from the ground state $1s^2 2s\ ^2S_{1/2}$ of the Li-like ions, then the orbital angular momentum of the initial ion state is equal to 0 ($L_i = 0$) and $l = l' = L_a$ [which cancels the Coulomb phase factor in Eq. (19)]. This approximation is reasonable considering that we will compare theoretical results with experimental data recorded at the EBIT, where it can be safely assumed, under the experimental conditions, that the largest population of Li-like ions is concentrated in the ground state. Moreover, since the quantization axis is taken along the direction of the electron beam, then $m_l = m_{l'} = 0$. Also, we consider electric-dipole transitions for which $j_{ph} = j'_{ph} = 1$, nonoverlapping resonances, and $J_a = J'_a$. Hence all sums over l, l'; j_{ph}, j'_{ph}; and J_a, J'_a vanish and the terms with reduced matrix elements and A_a cancel out in Eq. (19). Therefore, using angular-momentum algebra, we can carry out all needed summations and write down the elements of the photon density matrix ρ^{ph} corresponding to the dielectronic satellite transition s in the form

$$\rho^{ph}_{\lambda,\lambda'} = \frac{\sum_L B_L(s) \begin{pmatrix} j_{ph} & j_{ph} & L \\ \lambda & -\lambda' & -\Lambda \end{pmatrix} D^{(L)}_{\Lambda 0}(\cos\theta)}{2 \sum_L B_L(s) \begin{pmatrix} j_{ph} & j_{ph} & L \\ 1 & -1 & 0 \end{pmatrix} P_L(\cos\theta)}, \tag{22}$$

where P_L is a Legendre polynomial of order L and $B_L(s)$ is the so-called polarization moment of the ion,

$$B_L(s) = (-1)^{1 - J_f - S_a} (2L+1) \begin{pmatrix} l & L & l \\ 0 & 0 & 0 \end{pmatrix} \begin{Bmatrix} L_a & L & L_a \\ J_a & S_a & J_a \end{Bmatrix} \times \begin{Bmatrix} J_a & L & J_a \\ j_{ph} & J_f & j_{ph} \end{Bmatrix}. \tag{23}$$

Here { } are the 6-j symbols. It is interesting to note that $B_L(s)$ is defined completely by the mechanism of formation of the upper autoionization levels and in general has a very complicated form, which is simplified considerably under the assumptions we made above. The expression for $\rho^{ph}_{\lambda,\lambda'}$ in Eq. (19) is more general and independent of the form of $B_L(s)$, i.e., from the mechanism of the formation of upper autoionization levels by either dielectronic recombination or other atomic process.

In the helicity representation ρ^{ph} can be expressed in terms of the Stokes parameters [34]

$$\rho^{ph}_{\lambda,\lambda'} = \frac{1}{2} \begin{pmatrix} 1 + \eta_2 & -\eta_3 + i\eta_1 \\ -\eta_3 - i\eta_1 & 1 - \eta_2 \end{pmatrix}. \tag{24}$$

The degree of polarization is expressed in terms of Stokes parameters η_1, η_2, η_3 as

$$P = \sqrt{\eta_1^2 + \eta_2^2 + \eta_3^2}. \tag{25}$$

From Eqs. (19) and (20) it follows that the diagonal matrix elements $\rho^{ph}_{\lambda,\lambda}$ are equal to 1/2 and nondiagonal elements are equal to each other and equal to

TABLE I. Atomic and polarization characteristics for dielectronic satellite transitions $1s2s2p^2$-$1s^22s2p$ of Be-like Fe. λ are wavelengths, A_r are radiative probabilities, Q_d are intensity factors, E_a are autoionization energies, and P_0 are the values of maximum degree of polarization of transitions. Numbers in square brackets denote powers of 10.

Peak	Line	Ref. [38]	Transition	J_a-J_f	λ (Å)	A_r (s^{-1})	Q_d (s^{-1})	E_a (eV)	P_0
5	1	$E1$	$^3_2P-{}^3P$	1-2	1.86685	2.22[+14]	6.84[+13]	4751.6	0
6	2	$E2$	$^1D-{}^3P$	2-2	1.86795	1.41[+14]	7.00[+13]	4747.6	−1
	3		$^3S-{}^3P$	1-1	1.86835	8.75[+13]	3.23[+13]	4735.0	0
7	4	$E4$	^1S-^1P	0-1	1.86975	2.30[+14]	3.52[+13]	4775.3	0
	5	$E5$	^3S-^3P	1-2	1.87155	3.71[+13]	1.37[+13]	4735.0	0
	6	$E6$	^3D-^3P	1-1	1.87255	2.41[+14]	1.75[+14]	4719.9	−3/7
1	7	$E7$	^3_1P-^3P	1-0	1.87285	3.77[+14]	1.17[+14]	4715.2	3/5
	8	$E8$	^3D-^3P	2-1	1.87355	3.17[+14]	4.80[+14]	4716.5	1/3
	9	$E9$	^3_1P-^3P	2-2	1.87385	4.30[+14]	1.54[+14]	4726.8	−3/5
4	10	$E10$	^3_2P-^1P	2-1	1.87470	8.40[+13]	8.20[+13]	4756.3	3/5
	11	$E11$	^3D-^3P	1-2	1.87575	8.05[+13]	5.82[+13]	4719.9	3/41
2	12	$E12$	^3D-^3P	3-2	1.87585	2.30[+14]	6.62[+14]	4719.6	18/41
	13	$E13$	^3D-^3P	2-2	1.87675	8.17[+12]	1.24[+13]	4716.5	−3/7
3	14	$E14$	^3_1P-^3P	1-2	1.87715	1.00[+14]	3.11[+13]	4715.2	3/41
	15	$E15$	^1D-^1P	2-1	1.87814	1.45[+14]	1.48[+14]	4747.6	3/5
8	16	$E17$	^5P-^3P	3-2	1.88745	1.01[+13]	2.92[+13]	4679.1	18/41

$$\rho^{ph}_{1,-1}=\rho^{ph}_{-1,1}=-\frac{\eta_3}{2}. \tag{26}$$

Therefore, only one of Stokes parameters (η_3) is nonzero and equal to the degree of polarization P; thus

$$\eta_1=\eta_2=0,\ P=\eta_3. \tag{27}$$

Making use of Eqs. (19)–(27), the expression for the degree of polarization for a dielectronic satellite line s can be written as

$$P(s)=-\frac{\sum_L B_L(s)\begin{pmatrix} j_{ph} & j_{ph} & L \\ 1 & 1 & -2 \end{pmatrix} D^{(L)}_{20}(\cos\,\theta)}{\sum_L B_L(s)\begin{pmatrix} j_{ph} & j_{ph} & L \\ 1 & -1 & 0 \end{pmatrix} P^{(L)}(\cos\,\theta)}. \tag{28}$$

For electric-dipole transitions the sum over L in the numerator has only one term with $L=2$ and in the denominator two terms with $L=0$ and 2.

Thus the expression for the degree of polarization can be rewritten as

$$P(s)=-\frac{3\,\sin^2\theta B_2(s)}{2\sqrt{10}B_0(s)+(3\cos^2\theta-1)B_2(s)}. \tag{29}$$

If $B_2(s)=0$, then the line has a zero degree of polarization. For nonzero $B_2(s)$ the degree of polarization $P(s)$ is maximum for $\theta=90°$ and Eq. (29) can be reduced to the simple form

$$P_0(s)=-\frac{3}{2\sqrt{10}\dfrac{B_0(s)}{B_2(s)}-1}. \tag{30}$$

The results of the calculation of $P_0(s)$ are presented in the next subsection.

B. Atomic and polarization characteristics

In Table I the atomic characteristics, namely, wavelengths λ, radiative transition probabilities A_r, intensity factors Q_d, and autoionization energies E_a, used to calculate polarization-dependent spectra of Be-like Fe dielectronic satellite line spectra are listed. Also displayed in Table I is the degree of polarization of each dielectronic satellite line $P_0(s)$, which has been computed using the formalism discussed in Sec. II A. Atomic data have been calculated using the $1/Z$ perturbation theory and approximation for atomic structure calculations implemented in the MZ code [35,36]; autoionization energies E_a have been determined using the data from [37] and are schematically illustrated in Fig. 1. As it is seen in Fig. 1, to produce Be-like Fe dielectronic satellite lines the energy of the beam has to be in the range 4.665–4.775 keV. There are 16 lines listed combined into 8 peaks, which correspond to spectral features that can be identified in the present experimental spectra. For comparison, the lines in Table I are also labeled according to the notation of [38] where they were discussed in terms of their contribution to tokamak spectra. Peaks 4, 5, 7, and 8 are formed by single lines. All other peaks consist of more than one line. Relativistic effects are important for the Be-like Fe ion and intercombination lines, such as 2, 10, and 16, are intense. In

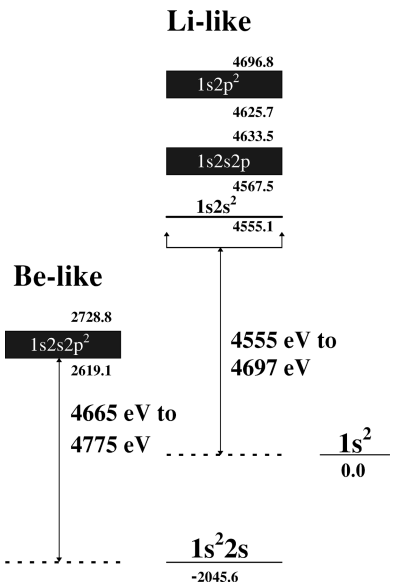

FIG. 1. Schematic energy-level diagram of the relevant Fe ionization stages. All the energies are measured with respect to the He-like Fe ground state. Each box represents groups of energy levels associated with a given configuration; energy bounds for the box are indicated. Also shown are the ranges of energies for resonant electron capture from the ground states of He- and Li-like Fe.

general, the lines contributing to the same peak have different magnitudes and signs of the degree of polarization P_0. According to Eq. (1), if the sign of P_0 is positive, the line is predominantly polarized parallel to the electron-beam axis, and if the sign of P_0 is negative, the line is predominantly polarized perpendicular to the electron-beam axis.

Since we are assuming that electron capture originates only from the ground level $1s^2 2s\ ^2S_{1/2}$ of Li-like Fe, then in the pure LS-coupling scheme autoionization levels associated with the configuration $1s2s2p^2$ and terms S and D can be populated, i.e.,

$$1s^2 2s\ ^2S_{1/2} + \kappa s \rightarrow 1s2s2p^2(s \text{ channel}), \tag{31}$$

$$1s^2 2s\ ^2S_{1/2} + \kappa d \rightarrow 1s2s2p^2(d \text{ channel}). \tag{32}$$

The corresponding transitions arising from these levels are lines 2–6, 8, 11–13, and 15 in Table I. All lines arising from terms populated via the s channel are unpolarized [see Eqs. (23) and (30)]. Hence lines 3–5 are unpolarized. The polarization of lines 2, 6, 8, 11–13, and 15 was calculated according to Eqs. (23) and (30). All other lines, i.e., 1, 7, 9, 10, 14, and 16, occur from levels associated with P terms, which, due to relativistic effects, are produced by mixing with S and D terms having the same J_a. There are two different ^3P terms corresponding to different intermediate momentum coupling. The terms ^3_1P and ^3_2P denote the intermediate momentum coupling $2p^2(^3P)2s(^2P)1s\ ^3P$ and $2p^2(^3P)2s(^4P)1s\ ^3P$, respectively. The mixing of terms S, D, and P within a complex described by the same parity and the same J_a increases with Z and becomes significant for the case of Fe ($Z=26$). All lines arising from levels with $J_a=0$ are unpolarized. Lines arising from nonzero J_a levels may show polarization. For $J_a=1$, the largest mixing coefficients for the level ^3_1P are equal to 0.8 (^3_1P), -0.57 (^3D), and -0.16 (^3S). For the level ^3_2P they are 0.7 (^3_2P), 0.67 (^3S), and 0.17 (^3_1P). For $J_a=2$ the largest mixing coefficients for the level ^3_1P are equal to 0.86 (^3_1P), 0.39 (^3D), and 0.27 (^1D). For the level ^3_2P they are 0.78 (^3_2P), -0.6 (^1D), and 0.12 (^3D). For $J_a=3$, only two levels are mixed, the mixing coefficients for the level ^5P are 0.98 (^5P) and -0.21 (^3D).

To calculate the polarization of lines arising from P terms, we selected the main term (S or D) depending on which makes the largest contribution to the level. This main term is then used to calculate the polarization of lines arising from P levels according to Eqs. (23) and (30). The largest neglected contribution to the polarization of the line due to this procedure is less than 2%. For example, level $^3_2P_1$ is described by an S main term, specifically $^3S_1$. Therefore, line 1 arising from $^3_2P_1$ is unpolarized. The other lines arising from P levels are polarized. The $^3_1P_1$ level is described mainly by a D term, specifically $^3D_1$. Two different lines 7 and 14 arise from this particular level. They have a different final lower level J_f and a different value of polarization. It should be mentioned that although lines 1 and 14 have the same upper level S_a, L_a, J_a and lower level J_f, they are described by different main terms. Thus lines 1 and 14 have different values of polarization. Line 14 has the same polarization as line 11, as their upper levels are described by the same quantum numbers, and the lower levels are also the same. The transitions from P levels with $J_a=2$ produce lines 9 and 10. Again, we have two P levels with the same quantum numbers but different intermediate momentum and different main terms. Specifically, the main term for $^3_2P_2$ is $^1D_2$. Hence, the polarization of line 10 arising from this level is the same as of line 15. The most complex case is observed for the level $^3_1P_2$, for which we have not one but two main D terms, namely, $^1D_2$ and $^3D_2$. This is taken into account in the calculation of polarization of line 9 arising from this level. The value of polarization of this line is in between the values of polarization of lines 2 and 13, having the same lower levels. The last line in Table I (i.e., line 16) arises from a P level with $J_a=3$. The main term for this P level is $^3D_3$. Hence the polarization of line 16 is the same as that of line 12. As was mentioned above, all upper levels of Be-like Fe considered here belong to the configuration $1s2s2p^2$, which is populated via s and d channels. One additional p-electron capture channel exists, which gives rise to energy levels associated with the configuration $1s2s^22p$. Since the autoionization energies of these levels are outside the range of electron-beam energies considered in this work, corresponding satellite line transitions were not taken into account.

In summary, it should be noted that Eqs. (23) and (30) are written for the case of pure LS coupling, but they are still valid in our case. First, we have only two channels of electron capture, which allowed us to treat the upper levels according to the way in which they were prepared. Thus we can calculate the polarization of lines arising from S and D levels. Second, in most cases we have only one main term for each P level; this allowed us to use the quantum numbers of the main term for the calculation of the polarization of lines arising from P levels.

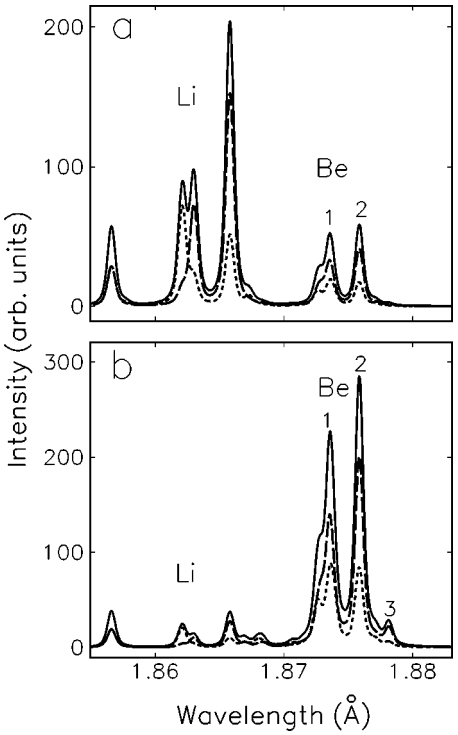

FIG. 2. Theoretical polarization-dependent spectrum of Li- and Be-like Fe calculated for two different energies of the electron beam: (a) $E_b = 4.698$ keV and (b) $E_b = 4.717$ keV. — — —, intensity associated with the parallel polarization state; · · ·, intensity associated with the perpendicular polarization state; ——, total intensity. Spectral features in Be are labeled according to the peak labeling of Table I. The Li spectral features were discussed in Ref. [30].

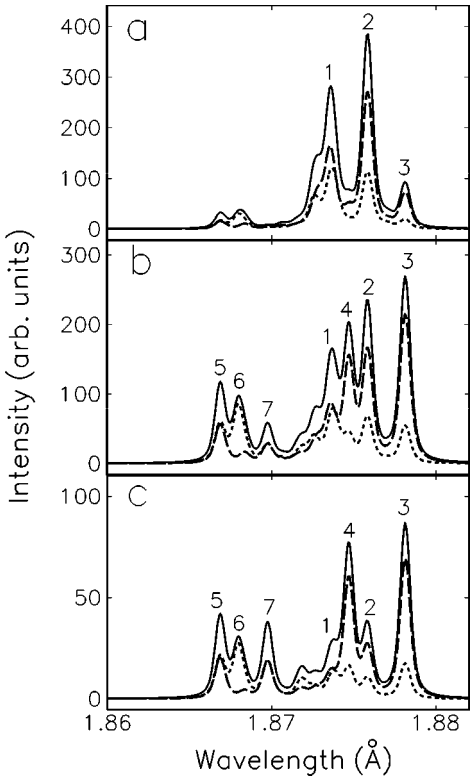

FIG. 3. Theoretical polarization-dependent spectrum of Be-like Fe calculated for three different energies of the electron beam: (a) $E_b = 4.734$ keV, (b) $E_b = 4.762$ keV, and (c) $E_b = 4.775$ keV. — —, intensity associated with parallel polarization state; · · ·, intensity associated with perpendicular polarization state; ——, total intensity. Spectral features are labeled according to the peak labeling of Table I.

C. Polarization-dependent spectra

Theoretical results for polarization-dependent spectra of dielectronic satellite lines in Be-like Fe are presented on Figs. 2(a), 2(b), 3(a), 3(b), and 3(c) calculated for five different energies of the electron beam: $E_b = 4.698$, 4.717 keV in Figs. 2(a) and 2(b), respectively, and $E_b = 4.734$, 4.762, and 4.775 keV in Figs. 3(a), 3(b), and 3(c), respectively; these energies are in the range of the autoionization energies listed in Table I. Since we compare synthetic polarization-dependent spectra with experimental spectra recorded at the LLNL EBIT (see Sec. III), theoretical results were calculated assuming electron-beam characteristics and line profiles suitable for the experimental conditions and instruments used at the LLNL EBIT, namely, the distribution of energies in the electron beam was modeled with a Gaussian function of 47 eV of full width at half maximum (FWHM). Line shapes were experimentally determined, approximated by numerical fits, and used to model line transitions. In particular, for the results presented in Figs. 2 and 3 we used Voigt line shapes of Voigt parameter $a = 0.7$ and FWHM equal to 0.5 mÅ. The Be spectral features (peaks) are labeled according to Table I.

The spectra displayed in Figs. 2 and 3 illustrate the main properties of the theoretical results: (i) the dependence of the spectra on the electron beam energy E_b and (ii) the polarization properties of the spectra. First, as the value of the electron-beam energy E_b increases different electron capture resonances are excited and the spectrum changes significantly. For $E_b = 4.698$ keV (lowest value considered here) some Li-like lines are still prominent; these lines were discussed in detail elsewhere [29,30]. Since the intensities of Li and Be lines are proportional to the populations of different ground states (He- and Li-like ions, respectively) the adjustment of their relative intensities is, to some extent, arbitrary. However, the intensities of all Be lines displayed in Figs. 2 and 3 are proportional to the Li ground-state population and the changes in total intensity distribution of the spectra reflect the dependence on E_b. As E_b increases, Be peaks 1 and 2 are the first ones to ''turn on'' and then 3–7 follow. For $E_b = 4.775$ keV (the highest value considered here) peaks 1 and 2 begin to ''turn off.'' Peak 4 consists of a single, polarized line (line 10) that is an intercombination line and due to relativistic effects is very pronounced in the Fe spectrum. Another strong intercombination line (line 2) is also prominent at high values of E_b, but it blends with unpolarized line 3 to form peak 6. Peaks 1–3 contain lines with the lowest values of E_a (see Table I) and can be observed when the Li-like emission becomes important, i.e., for electron-beam energies $E_b < 4.72$ keV. In general, lines with different degrees of polarization blend to give rise to peaks and the polarization properties of these spectral features can be traced back to those of their constituent lines.

Three traces are shown in Figs. 2 and 3, which represent the intensity distributions associated with the parallel polarization state, perpendicular polarization state, and their sum, i.e., the total intensity at 90°, calculated according to Eqs. (7) and (8). This way of presenting the results clearly shows the

relative contributions of parallel and perpendicular polarization states to the total intensity distribution and highlights those peaks (i.e., spectral features) that have significant polarization. The larger the difference between the intensity distributions associated with parallel and perpendicular polarization states, the larger the polarization of the peak. Peaks where the two traces are identical are unpolarized. Also, it is interesting to note the differences in relative intensity distributions associated with each polarization-dependent spectrum. This is clearly observed in peaks 2–4 and 6, which have strong polarization. The fact that the spectral intensity distributions for the parallel and perpendicular components are different is important and it can be used to develop polarization spectroscopic diagnostics of electron beams. For peaks 1, 5, and 7 parallel- and perpendicular-component intensity distributions lie closer to each other and hence these peaks have weak polarization. Note that while peaks 5 and 7 are made out of a single, unpolarized line each, peak 1 represents a blending of five lines with different degrees of polarization. Unpolarized spectral features in unresolved satellite structures can play the same role for cross normalization as unpolarized lines in the case of well-resolved, single-line spectra.

III. EXPERIMENTAL DETAILS AND MEASUREMENTS

The experimental spectra were collected at the LLNL EBIT. The operation of EBIT has been described in detail in previous articles and reviews [27,39]. Only the specific details relevant to the accumulation of the polarization-dependent Be-like Fe spectra will be discussed here. Two sets of spectra were accumulated simultaneously at each EBIT electron-beam energy, using two individual von Hámos spectrometer setups [40]. The spectrometers observed photons emitted along axes perpendicular to the electron beam axis and their dispersion planes were also normal to the electron-beam axis. One spectrometer used a LiF(220) crystal and the other one a LiF(200) crystal. Both crystals were bent to 30 cm radius, providing an instrumental resolving power of $\lambda/\Delta\lambda = 2200$ and 1500, respectively. These crystals were chosen because of appropriate integrated reflectivities $R_\perp$ and $R_\parallel$ for x rays polarized perpendicular and parallel, respectively, to the electron-beam axis, which in turn is parallel and perpendicular to the spectrometers dispersion plane in the present experimental setup. In particular, the relative reflectivity $R = R_\perp / R_\parallel$ indicates the polarization sensitivity of the crystal, as the intensity of the observed lines is given by the relationship

$$I_{obs} = R_\parallel I_\parallel + R_\perp I_\perp , \tag{33}$$

where $I_\parallel$ and $I_\perp$ are the x-ray intensities for polarization components parallel and perpendicular, respectively, to the electron-beam axis. Using crystals with very different values for R provides the most polarization sensitivity to the experiment. R is strongly dependent on the Bragg angle and on whether or not the crystal is perfect [41,42]. In fact, the relative reflectivity is described by $R = |\cos^m(\theta)|$, where θ is the Bragg angle and $1 \leqslant m \leqslant 2$. The characteristics of the two crystals used in this experiment and for the modeling are given in [42]. The LiF(220) crystal has a spacing of $2d = 2.848$ Å, corresponding to a nominal Bragg angle of 41° at the wavelengths of interest. The LiF(200) crystal has a spacing of $2d = 4.027$ Å, corresponding to a nominal Bragg angle of 27.50° at the wavelengths of interest. The relative reflectivities for the LiF(220) and the LiF(200) crystals were calculated to be $R_{220} = 0.12$ and $R_{200} = 0.56$ using the data of Ref. [42]. These values are close to those for perfect crystals. The use of these values seemed appropriate for the crystals we used, as they showed only a small degree of mosaic spread in x-ray topographic tests [24]. It is possible, however, that in the process of bending the crystals, the amount of mosaic spread has increased. This would have decreased the value of R. We did not test for this.

The spectrometers wavelength scales were calibrated using the wavelengths of the four well-known He-like Fe lines. These are the resonance line w, the magnetic quadrupole line x, the intercombination line y, and the forbidden line z, which represent transitions from the $1s2p\ ^1P_1$, $1s2p\ ^3P_2$, $1s2p\ ^3P_1$, and $1s2s\ ^3S_1$ states, respectively, to the $1s^2\ ^1S_0$ ground state. Also, the resonance line w was measured with both spectrometers and the recorded line shapes were used to model the individual lines in the Be-like spectra. The electron-beam energy was put on an absolute scale and its energy width determined by scanning the voltage of the electron-beam power supply from 4.79 to 4.90 kV. Spectra were gathered and the intensity of the well-isolated line j in Li-like Fe, corresponding to the transition $1s2p^2\ ^2D_{5/2} - 1s^2 2p\ ^2P_{3/2}$, was plotted as a function of the beam energy. The Auger energy of j is known to be 4.664 keV and allowed the calibration to be carried out. An offset of 170 eV between the nominal beam energy given by the power supply voltage and the actual beam energy was determined by this procedure. This offset is caused by the space-charge effect of the beam electrons [39] and it could be scaled for all other energies using the fact that it varies inversely as the square root of the beam energy. The energy width of the electron beam was estimated to be approximately 47 eV from the analysis of the variation of the intensity of line j with E_b. This procedure was also done for the Be lines $E6$ and $E7$ and a consistent value of the width was obtained. The data were collected at seven corrected electron-beam energies in the range 4.669–4.792 keV. The spectra, accumulated simultaneously by the two spectrometers, differ due to the different crystal relative reflectivities and reflection coefficients. The theoretical polarization-dependent intensities were then used to model the spectral intensity distributions for comparison with those observed by the spectrometers.

IV. COMPARISON OF THEORETICAL AND EXPERIMENTAL RESULTS

Figures 4–8 show the comparison between theoretical and experimental spectra. The five electron-beam energies indicated, i.e., 4.698, 4.717, 4.734, 4.762, and 4.775 keV, were the energies used to model the data. The top panel of each figure shows the spectrum obtained with LiF(220) crystal, which represents emission from an almost-pure parallel polarization state. The bottom panel shows the spectrum obtained with LiF(200) crystal. It represents emission from a

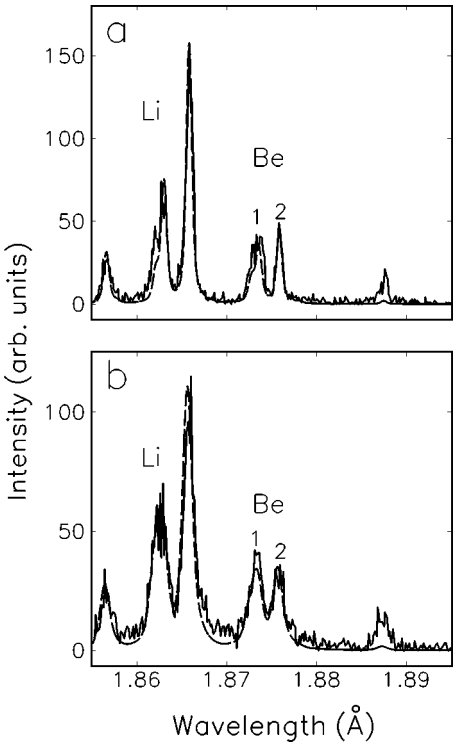

FIG. 4. Comparison of experimental spectrum (—) and theoretical spectrum of Li-and Be-like Fe (– – –) calculated at the electron-beam energy $E_b = 4.698$ keV associated with (a) an almost pure, parallel polarization state and (b) a mixture of polarization states.

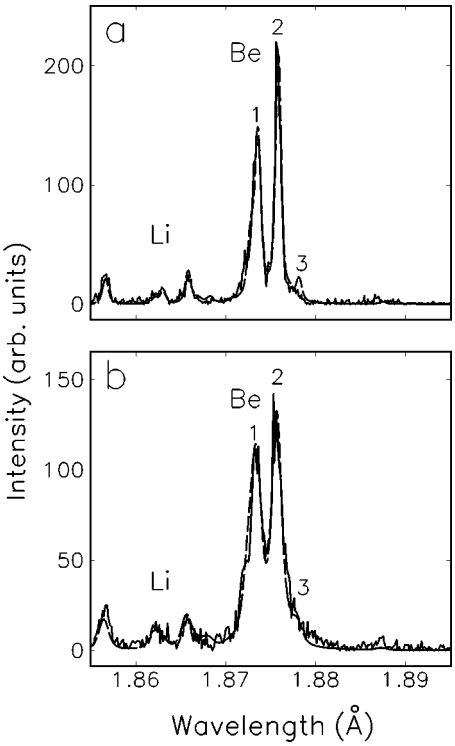

FIG. 5. Comparison of experimental spectrum (—) and theoretical spectrum of Li-and Be-like Fe (– – –) calculated at the electron-beam energy $E_b = 4.717$ keV associated with (a) an almost pure, parallel polarization state and (b) a mixture of polarization states.

mixture of both polarization states. As the electron-beam energy is increased, the observed spectra change significantly. The energy range was chosen to bracket maximum emission from Be-like Fe. As the value of E_b increases, different electron capture resonances can be excited and the spectral line emission changes. At the lowest energy Li-like ion lines are dominant (Fig. 4); at $E_b = 4.717$ keV there are some features due to Li-like ions, but they are smaller in comparison to lines from the Be-like ion (Fig. 5). As the energy increases, the Li-like lines vanish; however, starting at $E_b = 4.762$ keV, B-like ion lines appear and become very intense at $E_b = 4.775$ keV. An analysis of the B-like emission will be discussed elsewhere.

To aid the comparison, the theoretical spectra were convolved using a single Voigt profile (Voigt parameter $a = 0.7$ and FWHM equal to 0.5 mÅ) for the data recorded with the LiF(220) crystal and a double Voigt profile (both with parameters $a = 0.7$ and FWHM equal to 0.832 mÅ, but with a relative offset of 0.2 mÅ) for the LiF(200) crystal data. The values of the electron-beam energies used for producing the theoretical spectra were selected to produce the best agreement with the measurements. The values used were never more than ± 4 eV from the experimental value. This was justified considering comparable uncertainties in the experimental electron-beam energy and magnitude of the calculated resonance energies.

The agreement between theoretical and experimental spectra is overall very good. The agreement extends from a good reproduction of the energy dependence of the line

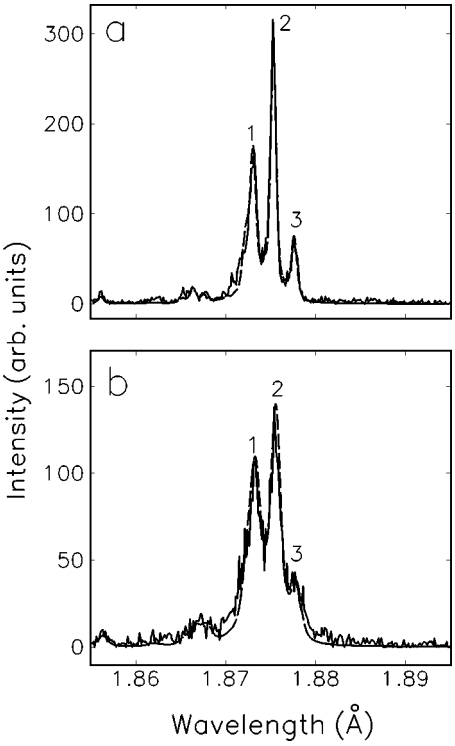

FIG. 6. Comparison of experimental spectrum (—) and theoretical spectrum of Be-like Fe (– – –) calculated at the electron-beam energy $E_b = 4.734$ keV associated with (a) an almost pure, parallel polarization state and (b) a mixture of polarization states.

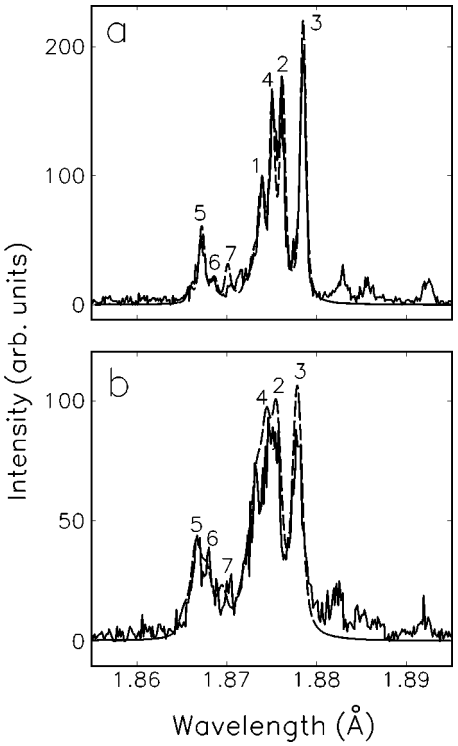

FIG. 7. Comparison of experimental spectrum (—) and theoretical spectrum of Be-like Fe (– – –) calculated at the electron-beam energy $E_b = 4.762$ keV associated with (a) an almost pure, parallel polarization state and (b) a mixture of polarization states.

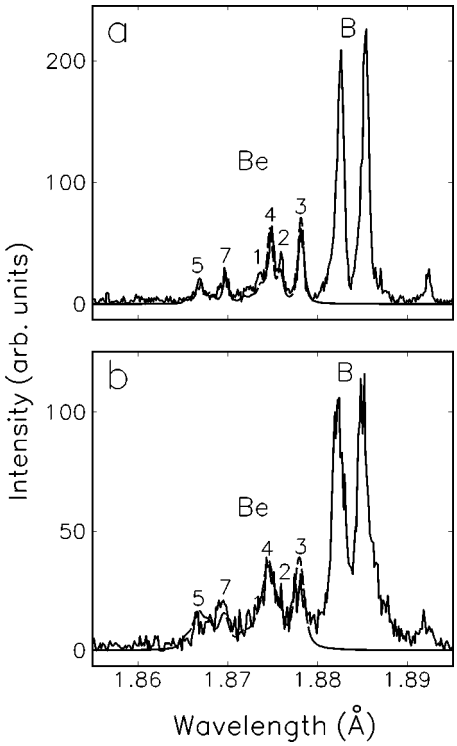

FIG. 8. Comparison of experimental spectrum (—) and theoretical spectrum of Be-like Fe (– – –) calculated at the electron-beam energy $E_b = 4.775$ keV associated with (a) an almost pure, parallel polarization state and (b) a mixture of polarization states.

emission, the line position, and the relative line intensities to the polarization-induced differences between the spectra from the two crystal spectrometers. This good agreement demonstrates that modeling of beam-excited, polarization-dependent spectra can be accomplished with confidence. Some disagreements can be noted, but these are for weak lines, for example, peak 1 in the LiF(200) spectrum of Fig. 4, peak 3 in the LiF(220) spectrum of Fig. 5, peak 7 in the LiF(220) spectrum of Fig. 7, and peaks 2–4 in the LiF(200) spectrum of Fig. 7.

Very important for developing polarization diagnostics is the good agreement between theoretical predictions and data for lines that are sensitive markers for polarized line emission. These include the pair of features labeled 1 and 2 and the pair labeled 5 and 6. The polarization sensitivity arises from the fact that these pairs are made up of lines with nearly opposite polarization properties. Peak 2 is comprised of two lines with positive polarization, while peak 1 contains five lines that on average are negatively polarized. Similarly, peak 5 consists of an unpolarized line, while peak 6 contains two lines that on average are strongly negatively polarized. Looking at Figs. 4–6, a clear difference in the observed intensity ratio of peaks 1 and 2 is seen when comparing the LiF(220) and LiF(200) spectra. The same is seen when looking at the ratio of peaks 5 and 6 in Fig. 7. This behavior is reproduced very well with our model calculations. The ratio of the two features in each pair can therefore be used as a clear marker for polarization.

V. SUMMARY AND CONCLUSIONS

We have studied theoretically and experimentally the polarization properties of dielectronic satellite lines of Be-like Fe ions excited by an electron beam. Using the photon density matrix formalism, we have calculated the degree of polarization of each dielectronic satellite line. Specifically, from a total of sixteen lines we found that four of them were unpolarized, while the other ones had different degrees of polarization either parallel or perpendicular to the electron-beam axis. Based on the calculated atomic and polarization characteristics of satellite lines and on the assumption of a Gaussian distribution function for the electron beam, we have computed the line intensity distribution associated with states of polarization parallel and perpendicular to the electron-beam axis. With these spectral distributions we have modeled the complex dielectronic satellite line spectra of Be-like Fe ions excited by an electron beam. We have compared our synthetic spectra with experimental measurements. The experimental data were collected at the LLNL EBIT using two crystal spectrometers that simultaneously recorded spectra over a range of electron-beam energy under identical experimental conditions. One spectrometer recorded an almost-pure polarization state spectrum, while the other one recorded a mixture of both components. The agreement between theoretical and experimental spectra is good at each electron-beam energy. This agreement confirms the good reproduction of the energy dependence of line emission and polarization sensitivity of the satellite spectra. Polarization markers have been identified, which can be used to infer

the presence of electron beams in low-density plasmas. In conclusion, the present work represents a test of the theoretical capability to model the polarization properties of complicated spectra excited by a low-density electron beam and sets a reference framework for developing polarization-based spectroscopic diagnostics relevant to more complicated systems such as plasmas.

ACKNOWLEDGMENTS

This work was supported by NSF, Grant No. OSR-9353227, a DOE-EPSCOR grant, and LLNL, Contract No. B336460. Work at LLNL was performed under the auspices of DOE under Contract No. W-7405-ENG-48 and was supported in part by the Office of Basic Energy Sciences, Chemical Sciences Division.

[1] S.C. Wilks, W.L. Kruer, M. Tabak, and A.B. Langdon, Phys. Rev. Lett. **69**, 1383 (1992).
[2] P. Gibbon, Phys. Rev. Lett. **73**, 664 (1994).
[3] A. Pukhov and J. Meyer-ter-Vehn, Phys. Rev. Lett. **76**, 3975 (1996).
[4] J.P. Matte, J.C. Kieffer, S. Ethier, M. Chaker, and O. Peyrusse, Phys. Rev. Lett. **72**, 1208 (1994).
[5] H. Ruhl, J. Opt. Soc. Am. B **13**, 388 (1996).
[6] M. Tabak, J. Hammer, M.E. Glinsky, W.L. Kruer, S.C. Wilks, J. Woodworth, E.M. Campbell, M.D. Perry, and R.J. Mason, Phys. Plasmas **1**, 1626 (1994).
[7] E. Haug, Sol. Phys. **61**, 129 (1979).
[8] E. Haug, Sol. Phys. **71**, 77 (1981).
[9] I. Percival and M.J. Seaton, Philos. Trans. R. Soc. London, Ser. A **251**, 113 (1958).
[10] M.K. Inal and J. Dubau, J. Phys. B **20**, 4221 (1987).
[11] A.S. Shlyaptseva, A.M. Urnov, and A.V. Vinogradov, P.N. Lebedev Physical Institute Report No. 194, 1981 (unpublished).
[12] A.V. Vinogradov, A.M. Urnov, and A.S. Shlyaptseva, in *Atomic and Ionic Spectra and Elementary Processes in Plasmas*, Proceedings of the P.N. Lebedev Physics Institute, Academy of Sciences of Russia, edited by I.I. Sobelman (Nova Science, Commack, NY, 1992), Vol. 192, p. 92.
[13] Y. Itikawa, R. Srivastava, and K. Sakimoto, Phys. Rev. A **44**, 7195 (1984).
[14] M.K. Inal and J. Dubau, Phys. Rev. A **47**, 4794 (1993).
[15] H.L. Zhang, D.H. Sampson, and R.D. Clark, Phys. Rev. A **41**, 198 (1990).
[16] K.J. Reed and M.H. Chen, Phys. Rev. A **48**, 3644 (1993).
[17] M.K. Inal and J. Dubau, J. Phys. B **22**, 329 (1989).
[18] M.H. Chen and J.H. Scofield, Phys. Rev. A **52**, 2057 (1995).
[19] A.S. Shlyaptseva, I.E. Golovkin, and U.I. Safronova, J. Quant. Spectrosc. Radiat. Transf. **56**, 157 (1996).
[20] V.A. Veretennikov, A.E. Gurei, A.N. Dolgov, V.V. Korneev, and O.G. Semenov, Pis'ma Zh. Éksp. Teor. Fiz. **47**, 29 (1988) [JETP Lett. **47**, 35 (1988)].
[21] J.C. Kieffer, J.P. Matte, H. Pepin, M. Chaker, Y. Beaudoin, C.Y. Chien, S. Coe, G. Mourou, and J. Dubau, Phys. Rev. Lett. **68**, 480 (1992).
[22] J.C. Kieffer, J.P. Matte, M. Chaker, Y. Beaudoin, C.Y. Chien, S. Coe, G. Mourou, J. Dubau, and M.K. Inal, Phys. Rev. E **48**, 4648 (1993).
[23] J.R. Henderson, P. Beiersdorfer, C.L. Bennet, S. Chantrenne, D.A. Knapp, R.E. Marrs, M.B. Schneider, K.L. Wong, G.A. Doschek, J.F. Seely, C.M. Brown, R.E. LaVilla, J. Dubau, and M.A. Levine, Phys. Rev. E **65**, 705 (1990).
[24] P. Beiersdorfer, D.A. Vogel, K.J. Reed, V. Decaux, J.H. Scofield, K. Widmann, G. Hölzer, E. Förster, O. Wehrhan, D.W. Savin, and L. Schweikhard, Phys. Rev. A **53**, 3974 (1996).
[25] P. Beiersdorfer, J. Crespo López-Urrutia, V. Decaux, K. Widmann, and P. Neill, Rev. Sci. Instrum. **68**, 1073 (1997).
[26] E. Takács, E.C. Meyer, J.D. Gillaspy, J.R. Roberts, C.T. Chantler, L.T. Hundson, R.D. Deslattes, C.M. Brown, J.M. Laming, J. Dubau, and M.K. Inal, Phys. Rev. A . **54**, 1342 (1996).
[27] R.E. Marrs, P. Beiersdorfer, and D. Schneider, Phys. Today **47** (10), 27 (1994).
[28] K.L. Wong, P. Beiersdorfer, K.J. Reed, and D.A. Vogel, Phys. Rev. A **51**, 1214 (1995).
[29] P. Beiersdorfer, T.W. Phillips, K.L. Wong, R.E. Marrs, and D.A. Vogel, Phys. Rev. A **46**, 3812 (1992).
[30] A.S. Shlyaptseva, R.C. Mancini, P. Neill, and P. Beiersdorfer, Rev. Sci. Instrum. **68**, 1095 (1997).
[31] I.I. Sobelman, L.A. Vainshtein, and E.A. Yukov, *Excitation of Atoms and Broadening of Spectral Lines*, edited by G. Ecker, P. Lambropoulos, I.I. Sobelman, and H. Walther, Springer Series on Atoms and Plasmas Vol. 15 (Springer, Berlin, 1995).
[32] B. Shore, Astrophys. J. **185**, 1205 (1969).
[33] V.B. Berestetskii, E.M. Lifshitz, and L.P. Pitaevskii, *Relativistic Quantum Theory I* (Nauka, Moscow, 1968).
[34] K. Blum, *Density Matrix Theory and Applications* (Plenum, New York, 1981).
[35] V.L. Vainshtein and U.I. Safronova, At. Data Nucl. Data Tables **21**, 49 (1978).
[36] U.I. Safronova, Phys. Scr. **T26**, 59 (1989).
[37] U.I. Safronova and A.S. Shlyaptseva, Phys. Scr. **54**, 254 (1996).
[38] P. Beiersdorfer, T.W. Phillips, V.L. Jacobs, K.W. Hill, M. Bitter, S. Von Goeler, and S.M. Kahn, Astrophys. J. **409**, 846 (1992).
[39] M.A. Levine, R.E. Marrs, J.N. Bardsley, P. Beiersdorfer, C.L. Bennett, M.H. Chen, T. Cowan, D. Dietrich, J.R. Henderson, D.A. Knapp, A. Osterheld, B.M. Penetrante, M.B. Schneider, and J.H. Scofield, Nucl. Instrum. Methods Phys. Res. B **43**, 431 (1989).
[40] P. Beiersdorfer, R.E. Marrs, J.R. Henderson, D.A. Knapp, M.A. Levine, D.B. Platt, M.B. Schneider, D.A. Vogel, and K.L. Wong, Rev. Sci. Instrum. **61**, 2338 (1990).
[41] A. Burek, Space Sci. Instrum. **2**, 53 (1976).
[42] B.L. Henke, E.M. Gullikson, and J.C. Davis, At. Data Nucl. Data Tables **54**, 181 (1993).